Cathodic Cleaning and Heat Input in Variable Polarity Plasma Arc Welding of Aluminum

The relationships between arc polarity, workpiece heating, oxide removal and weld size are quantified

BY P. W. FUERSCHBACH

ABSTRACT. For variable polarity plasma arc welding (VPPAW) of 1100 Al, it was found that the net heat input to the aluminum workpiece did not decrease as independent changes in polarity balance enabled the tungsten electrode to become the predominant anode in the alternating current arc. For the thin sheet edge welds made in this study, the independent parameters used to vary the arc current polarity balance were very effective in delivering a wide range of actual arc power polarity balance. The ratio of electrode positive polarity arc energy to the total arc energy ranged from as little as 0.03 to as high as 0.99. Despite this pronounced difference in arc polarity, no significant variation in the average arc efficiency (net heat input/arc energy) of 0.51 was found. Substantial heating of the workpiece during electrode positive polarity was attributed to field type emission of electrons from the low boiling point aluminum cathode. Unlike thermionic emission at the tungsten, field emission electrons do not cool the cathode.

While the actual arc efficiencies were relatively constant, there were significant differences in the measured heat input, the weld size, and the effectiveness of the cathodic cleaning. Increases in the arc voltage resulted in a gradual increase in arc power as the aluminum workpiece became the primary cathode. This resulted in an increase in the measured heat input to the part and an increase in the melted volume. Despite variations in melted volume, no correlation between arc polarity and weld dimensions was observed. The effectiveness of positive polarity arc power in removing the surface oxide was clearly apparent when examining the resulting welds. Cleaning (*i.e.*, removal of the oxide) can be effectively controlled and optimized through proper selection of the independent parameters used to create the test weld matrix.

P.W. FUERSCHBACH is with Sandia National Laboratories, Albuquerque, N.Mex.

Introduction

The use of alternating current (AC) in arc welding permits the thorough removal of the tenacious surface oxide on aluminum at the welding station and in real time. Cathodic cleaning (Ref. 1) is the stripping of oxide from the metal surface during the part of the AC cycle when the workpiece is the cathode (electrode positive polarity) in the welding arc. Despite its importance to the welding industry, this oxide removal mechanism is not well understood.

Several theories (Ref. 2) have heen proposed to explain the field type emission that occurs in arcs from non-thermionic cathodes such as aluminum. Recent work (Refs. 3, 4) has supported the mechanism proposed by Druvesteyn (Ref. 5) that positive ions collect on the surface of the metal oxide creating a high electrostatic field. The thin oxide insulator breaks up in the presence of this field type emission, which encourages the observed wandering of the cathode spots across the workpiece surface. The dielectric oxide's presence is actually useful with low boiling point metals like aluminum as it contributes to arc stability (Ref. 6). In a similar manner, the addition of oxygen to argon shielding gas leads to the formation of a stable cathode root on the workpiece in gas metal arc welding.

KEY WORDS

Arc Efficiency
VPPAW
Calorimetry
Edge Weld
Cold Cathode
Electric Arc
Field Emission
Melt Efficiency
Oxide Removal
Arc Polarity

$$\eta = \frac{q_i}{q_o} \qquad (1)$$

Our understanding of energy transfer in aluminum welding is also incomplete. Arc efficiency (Ref. 1) is defined as the ratio of the net workpiece input power q_i, to the arc output power, q_o. Values of arc efficiency for nonconsumable electrode positive and alternating polarity welding processes are not well known. Conventional wisdom for aluminum arc welding states that the net heat input to the workpiece is dependent on the arc polarity balance. It is thought that when the tungsten electrode is the cathode (electrode negative polarity) a substantially larger fraction of the arc energy is transferred to the workpiece than when the tungsten is the anode.

Power supplies have been developed to vary the polarity balance in the AC waveform, and thereby achieve optimum cleaning and melting (Refs. 7–9). Power supply manufacturers suggest that the fraction of arc energy transferred to the workpiece can be dialed in through adjustment of the polarity balance. In this way, satisfactory removal of the alu-

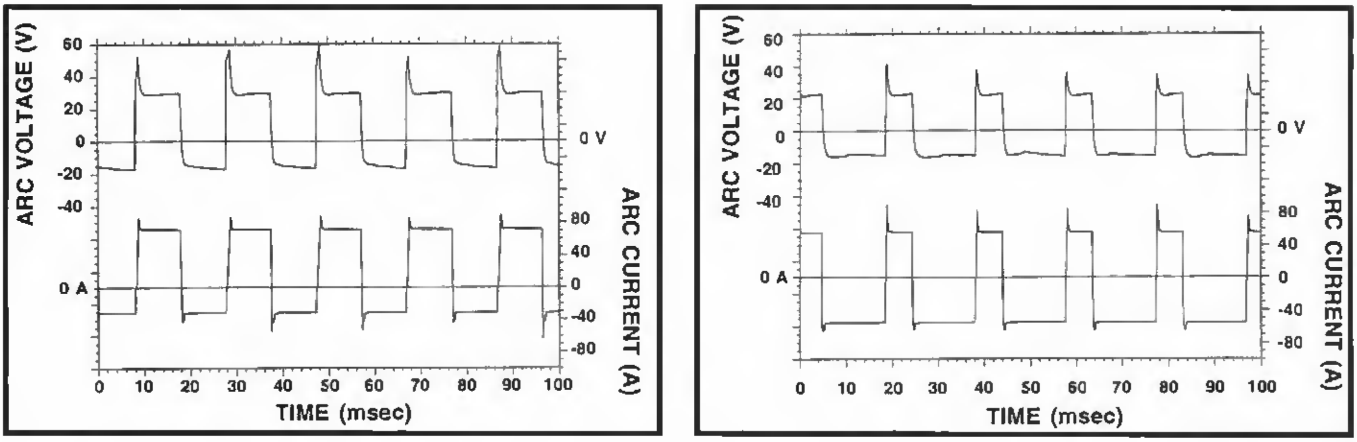

Fig. 1 — Typical voltage and current traces as recorded during the experiment: A — β = 0.3, θ = 0.5, $(Q_-)/(Q_t)$ = 0.19, B — β = 0.5, θ = 0.7, $(Q_-)/(Q_t)$ = 0.59.

minum oxide can be obtained along with optimum heating of the workpiece metal. In this study, calorimetric measurements were used to determine what effect polarity balance has on the heat input to the workpiece. By varying the polarity balance in a systematic way, and by measuring the arc power, the importance of process parameters on cathodic cleaning were investigated. It is hoped that quantifying the effects of variable polarity will lead to better models of the process and improved process understanding and control.

Experimental Procedure

Variable polarity plasma arc welds were made on 1.27 x 25 x 114 mm machined test specimens of 1100 aluminum. Two such pieces were joined in a standing edge weld geometry. The specimens were acid cleaned by a process described in Table 1. Four identically prepared specimens of 304L stainless steel also were welded in the experiment to test for dependence of arc efficiency on base material.

The welding power supply was built[1] for automated variable polarity plasma arc welding (VPPAW) and permits the independent selection of current amplitude (up to 200 A) and duration for both positive and negative polarity. The power supply achieves stable reignition during the positive half cycle by means of a 400-V open circuit potential. Both the arc current and voltage were recorded on a high-speed digital oscilloscope, which enabled the determination of the actual arc power during both the positive and negative cycles. Because of the high open circuit voltage, a special instrumentation unit was fabricated to permit fast response, yet isolated, oscilloscope measurements of the complete arc current and voltage waveform. Typical current and voltage traces are shown in Fig. 1A, B. The initial current spike at the beginning of each pulse is a feature of the power supply that was set to the minimum value. An arc power trace was obtained for each weld by multiplying the current and voltage waveforms together. Integration of the resulting power trace yielded a measure of total arc energy.

The net heat input to the workpiece was measured using a Seebeck envelope calorimeter in the manner described in Ref. 10. A CNC X-Y table translated the calorimeter and weld specimen under the welding torch. The calorimeter was left open during welding and closed immediately after welding was completed. The calorimeter walls were maintained at room temperature with a constant temperature bath. The calorimeter operates on the gradient layer principle and produces a voltage output that is proportional to the flux through the walls during the time required for the weld samples and fixture to cool to room temperature. The energy losses with this experimental technique due to radiation, convection, and evaporation have been estimated to be 1% or less of the arc energy. The calorimeter was calibrated for this study using the transient method described in Ref. 11.

In order to examine the effect of polarity balance on oxide removal, an experimental strategy was sought, that would vary arc polarity but also produce welds of similar size. For pulsed direct current gas tungsten arc welding (GTAW), root mean square (RMS) current has been shown (Ref. 10) to be a better indicator of weld heat input than average current, which is calculated as follows:

$$\text{Average Current} = \frac{|I_{(-)}|t_{(-)} + I_{(+)}t_{(+)}}{t_{(-)} + t_{(+)}} \qquad (2)$$

Table 1 — Aluminum Cleaning Procedure*

Step 1	Scrub each part with Alconox (alkaline detergent) and water. Rinse in deionized (DI) water. Hang to air dry.
Step 2	Immerse in alkaline non-etch (3.25 L DI, 209 mL Na_2SiO_4, 156 g Na_2Co_3, for 5 min. Rinse in DI water. Hang to air dry.
Step 3	Immerse in acid DeOx (3.5 L DI, 251 mL HNO_3, 105 g $NaBrO_4$) for 5 min. Rinse in DI water. Hang to air dry. Let parts stand 72 hours before welding.

*This procedure cleans and stabilizes the oxide on the surface of the weld sample.

Root mean square current is known to weight peak current amplitude to a greater degree and thereby compensates for the increased voltage and power that occurs during pulsing. In AC welding, high voltages are known to occur during the rapid arc current reversal. To help offset the greater arc powers that result from the higher voltages, a matrix of weld conditions that kept the RMS current constant was developed for this experiment. This approach enabled a large range of variations in polarity balance to be achieved while still achieving practical welds. Root mean square current is calculated from the following equation:

$$\text{RMS Current} = \sqrt{\frac{I^2_{(-)}t_{(-)} + I^2_{(+)}t_{(+)}}{t_{(-)} + t_{(+)}}} \qquad (3)$$

where $I_{(-)}$ is the current amplitude during the electrode negative portion of the cycle, $t_{(-)}$ is the time duration for elec-

1. MacGregor Welding Systems, Mildenhall, Suffolk, England.

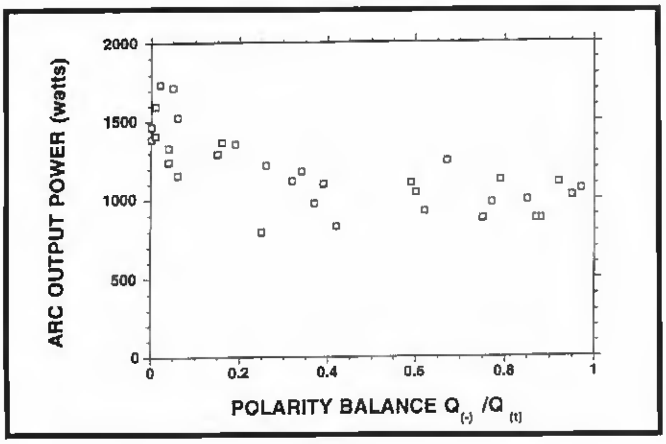

Fig. 2 — Effect of arc polarity balance on the measured arc power for VPPAW.

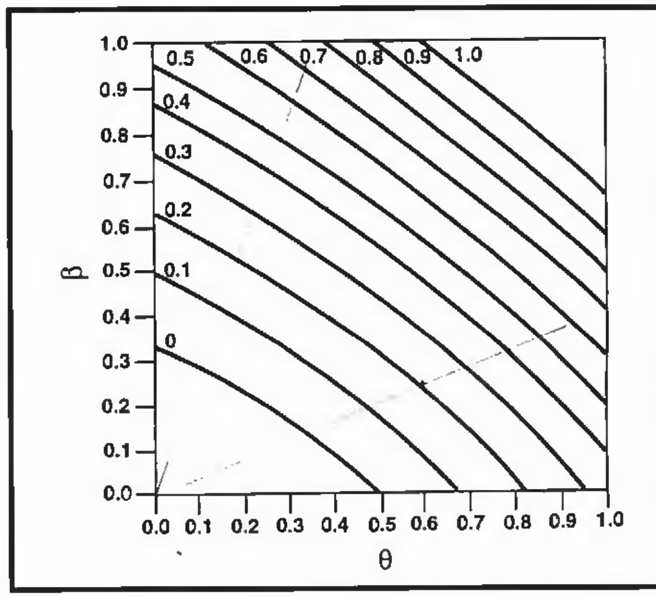

Fig. 3 — Effect of independent polarity parameters on the dependent polarity balance. The contour lines represent measured values of polarity balance. $R^2 = 0.94$.

trode negative, $I_{(+)}$ is the current amplitude for electrode positive, and $t_{(+)}$ is the time duration for electrode positive.

To vary polarity halance in a systematic way, two dimensionless parameters, β and θ, were used to produce the matrix of experimental conditions. The parameter β represents the electrode negative polarity fraction of the arc current. This parameter was first used by Okada (Ref. 9) in a similar study where only the current amplitude was varied. It is defined as follows:

$$\beta = \frac{|I_{(-)}|}{|I_{(-)}| + |I_{(+)}|} \tag{4}$$

The parameter θ indicates the electrode negative polarity duty cycle. It represents the fraction of arc time that the tungsten electrode is at negative potential. It is defined as:

$$\theta = \frac{t_{(-)}}{t_{(-)} + t_{(+)}} \tag{5}$$

Five levels (0.1, 0.3, 0.5, 0.7, 0.9) were chosen for both β and θ. The potential combinations with these two parameters resulted in a matrix of 25 unique weld conditions. Experimental trials indicated that an RMS current of 55 A would yield practical welds on these edge weld samples for each condition in the matrix. The current amplitudes $I_{(-)}$ and $I_{(+)}$, and the corresponding levels of β and θ for each condition are given in Table 2. Welds were made at 55 A RMS for each condition in Table 2, with replicates made of the welds marked with an asterisk.

Several other welding variables were held constant in the experiment in order to more directly observe the specific effects of arc polarity. The polarity reversal frequency was set at 50 Hz, a level that is common to many welding power supplies. Weld travel speed was held constant at 19.0 mm/s, a level consistent with high productivity automated welding applications. The especially important plasma torch setup conditions were not varied in the experiment either. Torch conditions are given in Table 2. Helium was used as a shielding gas because it is thought to restrict the cathodically cleaned area closer to the fusion zone region (Ref. 12).

Table 2 — Matrix of Experimental Conditions

β	θ	0.1 $t_{(-)} = 0.002$ $t_{(+)} = 0.018$	0.3 $t_{(-)} = 0.006$ $t_{(+)} = 0.014$	0.5 $t_{(-)} = 0.010$ $t_{(+)} = 0.010$	0.7 $t_{(-)} = 0.014$ $t_{(+)} = 0.006$	0.9 $t_{(-)} = 0.018$ $t_{(+)} = 0.002$
0.1	$I_{(-)}$	* 6.4	7.3	* 8.6	11.0	* 18.3
	$I_{(+)}$	57.9	65.6	77.3	99.0	165.0
0.3	$I_{(-)}$	* 24.6	27.1	30.6	36.0	45.8
	$I_{(+)}$	57.4	63.3	71.5	84.0	106.8
0.5	$I_{(-)}$	55.0	* 55.0	* 55.0	55.0	55.0
	$I_{(+)}$	55.0	55.0	55.0	55.0	55.0
0.7	$I_{(-)}$	106.8	84.0	* 71.5	* 63.3	57.4
	$I_{(+)}$	45.8	36.0	30.6	27.1	24.6
0.9	$I_{(-)}$	165.0	99.0	* 7.3	65.6	57.9
	$I_{(+)}$	18.3	11.0	8.6	7.3	6.4

Note — Experimental conditions replicated are marked with an *.

All welds were cross-sectioned in four places and examined with optical metallography. Penetration and cross-sectional area measurements were taken from the average of the four sections. Surface roughness measurements of the completed welds were made with a TMA Technologies microscan scatterometer (Ref. 13). This instrument is typically used to quantify the condition of mirror finishes by measuring the light reflected from a 670-nm wavelength laser diode source. The top of the fusion zone for each weld was examined in four places and the measured values were averaged.

Results and Discussion

Polarity Balance

Since actual arc energy will necessarily be affected by the uncertain arc voltage required to reignite the aluminum cathode, it is only practical to truly determine polarity balance for an experimental condition after the weld has been completed. The ratio of the negative polarity energy (Q_-) to the total arc energy (Q_t) has been calculated from the oscilloscope waveforms and will be referred to as polarity balance (Q_-)/(Q_t). Actual measured polarity balance values are plotted in Fig. 2 vs. the corresponding

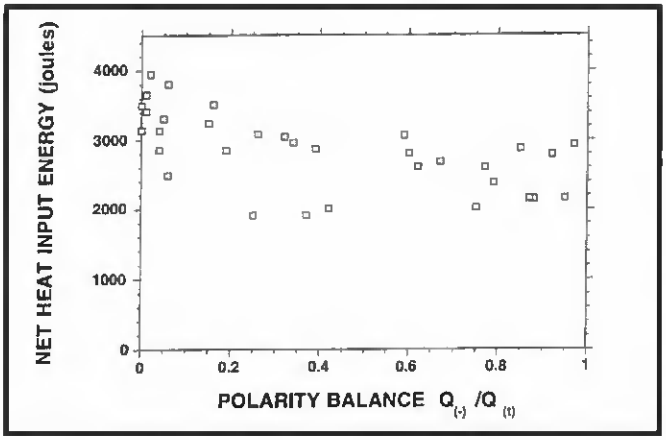

Fig. 4 — Effect of arc polarity balance on the calorimetrically measured heat input to the part.

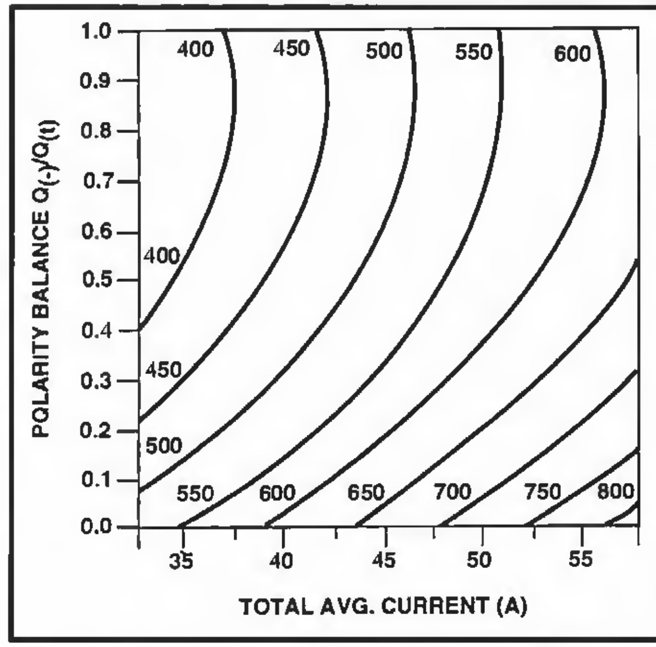

Fig. 5 — Effect of total average current and polarity balance on net input power. The contour lines represent net input power in watts. $R^2 = 0.88$.

measured total arc output power. As can be seen in the figure, the experimental design using the independent parameters β and θ was very effective in obtaining a wide range of electrode negative and electrode positive polarity conditions. The gradual increase in arc power that is seen at low levels of negative polarity balance can be attributed to an increase in the arc voltage, which occurred because aluminum was the predominant cathode. Low boiling point metals are poor thermionic emitters and higher arc voltages are required for breakdown when they become the cathode (Ref. 2).

The relationship between the dimensionless parameters β and θ, and the dependent polarity balance, also can be seen on the contour plot in Fig. 3. The contour lines delineate values of polarity balance. Recalling that low values of β and θ represent conditions that produce positive polarity, one can see from Fig. 3 that the polarity balance 0.1 contour line intercepts the θ axis at 0.67 and the β axis at 0.49. This indicates that, by itself, higher values of θ are required to achieve the same polarity balance as a given value of β by itself. Again this is due to the uncontrolled effect of arc voltage. Low levels of β will result in increased arc voltages due to the high positive current amplitudes that result from these conditions.

Arc Efficiency and Workpiece Heat Input

Measurements by several researchers in recent years have clearly demonstrated that in electrode negative polarity GTAW, 70 to 80% of the arc energy is transferred to the anode (Refs. 10, 14, 15). This arc efficiency is independent of the current amplitude since electron condensation is the primary source of energy transfer. For electrode negative polarity plasma arc welds, the fraction of arc energy transferred to the anode workpiece has been shown to vary from about 50 to 80% depending on the current amplitude and nozzle diameter. The slightly lower arc efficiencies for PAW have been attributed to partial arc energy transfer to the water-cooled torch nozzle (Ref. 10). For variable polarity GTAW or PAW, published arc efficiency values are not available, but making the tungsten the anode a high percentage of the time is believed to strongly decrease heat transfer to the workpiece (Ref. 16).

The wide range of polarity balance that was obtained in this experiment did not result in a consistent variation in heat transfer to the workpiece. The relative insensitivity of workpiece heat input to the arc polarity balance is shown in Fig. 4. One can see that the net arc energy absorbed by the edge weld samples does not depend on whether the tungsten electrode or the aluminum workpiece is the emitting cathode. The noticeable rise in net heat input at low polarity balance is readily explained by the increased arc output shown in Fig. 2.

Although net heat input does not appear to vary systematically with arc polarity, the net heat inputs measured in this experiment do vary significantly. The experimental design strategy of keeping RMS current (Equation 3) constant in order to produce welds of similar size was not particularly effective. An important goal for a study of this kind is to determine independent parameters that can be used in models to predict net heat input and the resulting weld size for real production applications. While RMS current was kept constant in this study, the experimental design allowed total average current (Equation 2) to vary from about 33 to 55 A. These small changes in average current were significant. The combined effect of changes in average current and in polarity balance on the net heat input can be seen in Fig. 5. The contours represent net power into the workpiece. It was surprising to see that the net power depends strongly on the total average current (*i.e.*, both electrode negative and electrode positive polarity) for all conditions.

It is also apparent from Fig. 5 that at values greater than approximately 0.4, polarity balance has a decreasing effect on net heat input. Again, this can be attributed to the uncontrolled effect of arc voltage on heat input that was shown in Fig. 4. If not for the variation in arc voltage, average current would be the sole indicator of net heat input.

The measured arc efficiency values shown in Fig. 6 further indicate that arc polarity has no consistent effect on energy transfer to the workpiece. The levels of arc efficiency given in the figure vary between 0.41 and 0.62 with an average efficiency of 0.51. These levels are somewhat lower than the values for electrode negative polarity PAW given above.

Note that the arc efficiencies measured for the four stainless steel welds are also plotted in Fig. 6. Despite the large difference in material properties between stainless steel and aluminum, the measured arc efficiencies are similar. The arc

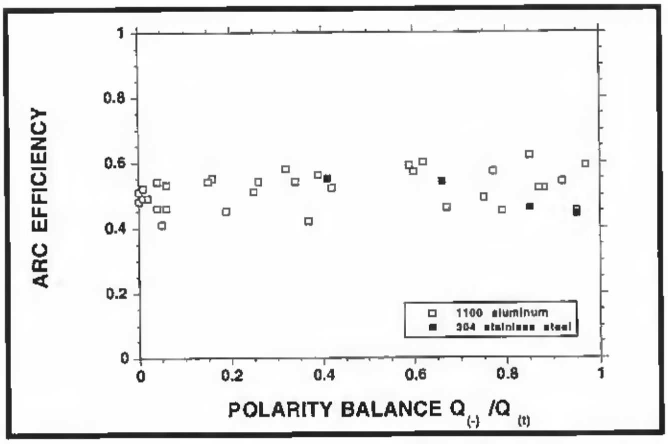

Fig. 6 — *Lack of correlation between the energy transferred to the part and the VPPAW arc polarity.*

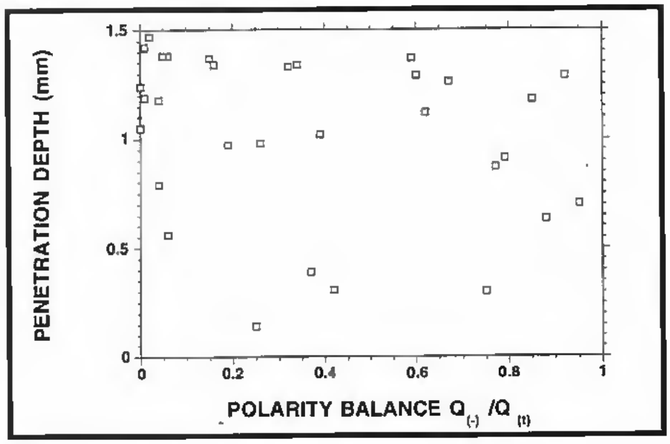

Fig. 7 — *Lack of correlation between weld penetration and arc polarity for VPPAW of 1100 Al.*

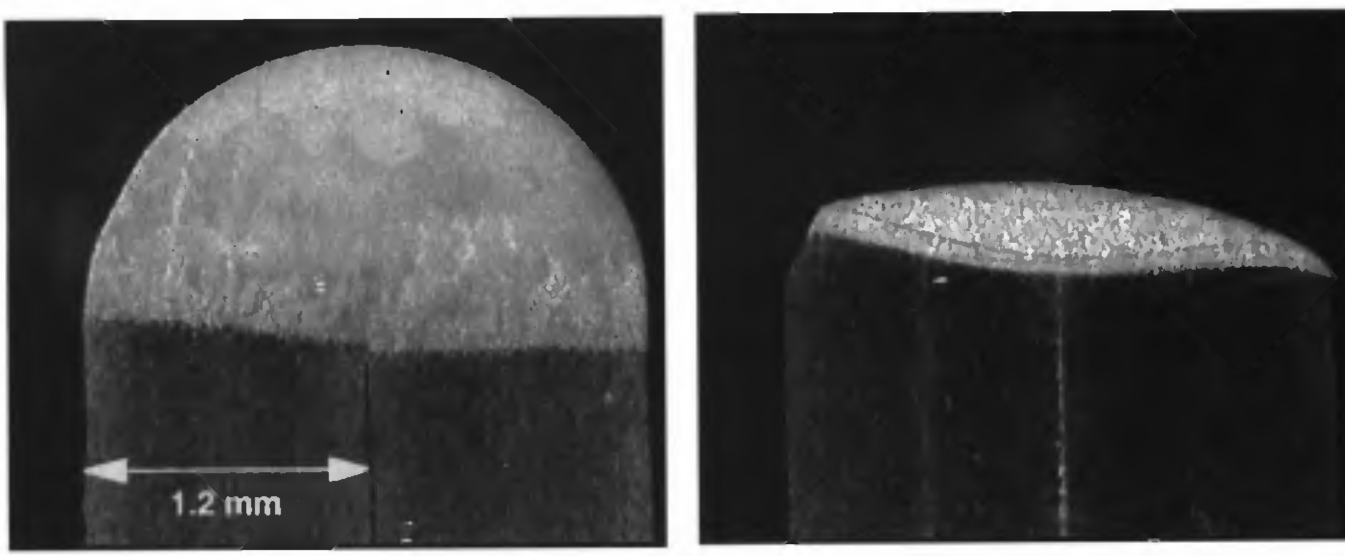

Fig. 8 — *Metallographic cross-sections of 1100 Al welds showing variation in melting for different conditions of polarity balance. A —* $Q_{(-)}/Q_{(t)} = 0.34$, $\beta = 0.5$, $\theta = 0.5$, $q_i = 630W$, $q_o = 1180W$; *B —* $Q_{(-)}/Q_{(t)} = 0.75$, $\beta = 0.9$, $\theta = 0.3$, $q_i = 430W$, $q_o = 880W$.

efficiency for variable polarity PAW does not appear to be influenced by these workpiece metals or the presence of different type oxides. Unlike thoriated tungsten, aluminum and iron are not considered to be thermionic cathodes because of their low boiling point, and field type emission from these metals is expected (Ref. 17). Field emission is simply the extraction of electrons from the cathode by the action of a strong electric field at the cathode surface (Ref. 18).

Energy Losses from the Tungsten

Recall from Equation 1 that arc efficiency in this experiment is determined by the ratio of the net input power measured by the calorimeter, q_i, to the arc output power measured with the oscilloscope, q_o. Losses to the torch electrode collet, the copper nozzle and the surroundings are not measured and should account for the substantial remaining fraction of arc energy that is not deposited at the workpiece. Conventional wisdom suggests these losses may be even greater during electrode positive polarity to offset an expected increase in tungsten heating when it becomes the anode.

The high levels of arc efficiency shown for low polarity balance in Fig. 6 surprisingly do not indicate decreased workpiece heating during electrode positive polarity. One possible explanation is that energy transfer to the tungsten anode is of the same degree as when the workpiece is the anode, but that lower net energy transfer to the tungsten is reduced by losses from the tungsten back to the workpiece. Two likely ways that energy at the tungsten could be transferred back again to the workpiece are convective losses to the gas, and radiative losses from the electrode. Estimates of the magnitude of these potential losses will now be made.

Cooling of an electrode negative GTAW workpiece anode by a transpiring gas has been demonstrated by Schoeck and Eckert (Ref. 19). Their experiments clearly indicate that gas flow away from the anode can feed significant amounts of arc energy back to the cathode. During electrode negative polarity VPPAW, heat transfer to the workpiece anode is aided by the shielding gas flow, which in a typical welding torch is directed toward the weld pool. One might expect that heat input to the tungsten anode in an electrode positive polarity arc might be reduced because the gas flow is in the direction opposite to the electron flow and may serve to transfer some heat back from the electrode to the workpiece. Convective heat transfer between the tungsten

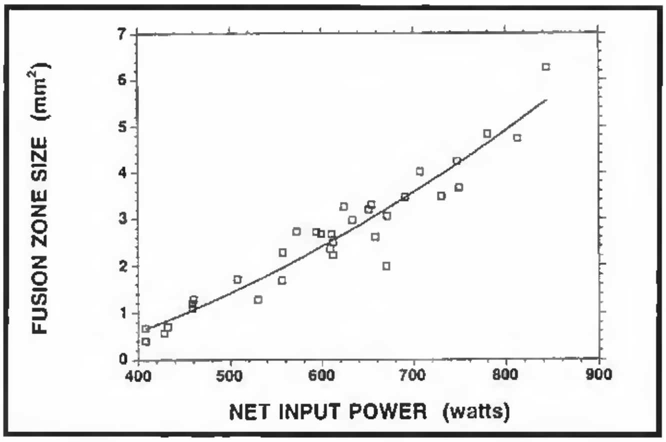

Fig. 9 — Fusion zone size variation as a function of calorimetrically determined absorbed power.

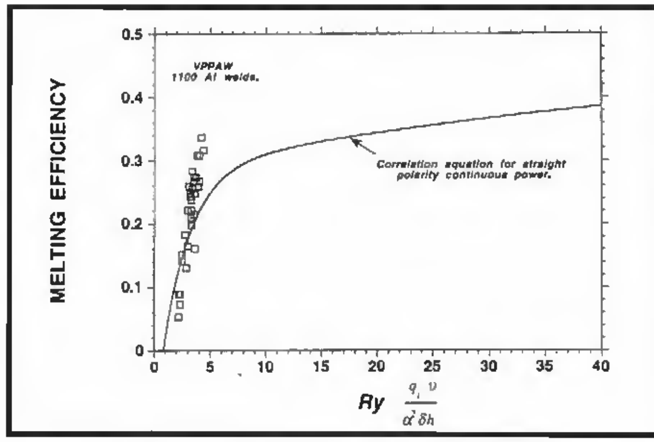

Fig. 10 — Comparison of VPPAW Al melting efficiencies with equation for continuous power PA and GTA welds on Ni 200 and 304 stainless steel.

Table 3 — Plasma Torch Setup

PAW torch	Thermal Dynamics PWM-3A
Orifice nozzle	2.0 mm dia.
Orifice gas	Argon @ 0.50 lpm
Shielding gas	Helium @ 9 lpm
Tungsten electrode	3.2 mm dia. 1.5% La_2O_3
Pilot current	10 A continuous
Nozzle stand-off distance	1.3 mm

electrode and the orifice gas can be estimated using Newton's law of cooling:

$$q_{conv} = hA(T_s - T_\infty) \quad (6)$$

where q_{conv} is the power transferred to orifice gas, h is the film coefficient, A is the surface area of the tungsten, and T_s is the temperature of the tungsten surface and T_∞ is the free stream gas temperature. Postweld examination of the tip of the tungsten electrode revealed that the tip had melted and become almost spherical during the variable polarity arc. To calculate the film coefficient, we will use a dimensionless parameter correlation (Ref. 20) for flow over a sphere:

$$Nu = 2 + 0.6\, Re^{0.5} Pr^{0.33} = \frac{hD}{k} \quad (7)$$

Where Nu = Nusselt number; Pr = Prandtl number of the orifice gas; Re = Vd/v = Reynolds number of the orifice gas; V = gas flow velocity at the anode; D = diameter of the spherical tip; k = thermal conductivity of the orifice gas; v = kinematic viscosity of the orifice gas.

Due to the constricting orifice, the gas velocities surrounding the tungsten electrode can be substantial in a plasma arc torch. Using room temperature values for the properties of the orifice gas, and V = 26.3 m/s, Re was estimated to be 17900, Nu = 73.4, and h = 406 W/m²K. If we assume worst case, that the tungsten tip is at its melting point 3410°C and the orifice gas is 20°C, substituting into Equation 6 yields q_{conv} = 44 W. While a significant temperature difference may exist for convective cooling, the relatively low value of power transferred to the orifice gas can be simply explained by the small surface area of the anode. With the VPPAW process, convective losses from the tungsten do not appear sufficient to retransfer substantial energy from the anode back to the cathode, unlike the experiment of Shoeck and Eckert.

The second type of possible loss from the tungsten back to the workpiece is radiative transfer. An upper estimate for the radiative losses q_{rad} from the tungsten electrode tip can be made assuming that the tungsten electrode tip is convex and completely enclosed by the copper orifice, which is concave. From the Stefan-Boltzman law:

$$q_{rad} = \sigma A_e \varepsilon_e \left(T_e^4 - T_n^4\right) \quad (8)$$

where σ is the Stefan-Boltzman constant, A_e is the electrode surface area, ε_e = 0.39 is the emissivity of the tungsten, T_e is the melting point of tungsten, and T_n is the temperature of the copper orifice. A conservative estimate for radiative loss based on a room temperature value for T_n is q_{rad} = 96W. This value is probably conservatively high since with the small field of view, most of the radiative losses from the tungsten will not reach the workpiece and will likely be absorbed by the copper orifice. When compared with the arc powers given in Fig. 2, it seems unlikely that significant amounts of energy can be radiatively transferred from the tungsten anode to the workpiece.

The magnitude of convective and radiative losses from the tungsten back to the workpiece are insufficient to reasonably explain the high arc efficiencies obtained during electrode positive polarity. Since we know that in electrode positive polarity a large fraction of arc energy is deposited at the cathode workpiece, and that substantial losses from the anode back to the workpiece are improbable, we must conclude that the energy never reaches the tungsten anode.

Significance of the Cathode Material

To reconcile substantial workpiece heating during electrode positive polarity, it is instructive to consider an electrode negative polarity GTAW or VPPAW torch where we know that most of the arc energy is typically transferred to the workpiece. There are three regions in an electric arc where a substantial voltage drop occurs and thereby energy is exchanged. In the main arc column, a relatively small electric field intensity exists where small amounts of power are dissipated as radiative and convective losses from the hot plasma to the surroundings. The energy exchanged here depends primarily on the length of the column and is considered to be minor for welding arcs. It is in two narrow regions close to the electrodes where the field intensity increases substantially, the anode fall, and the cathode fall, that significant electrical energy is transferred. The thermal gradients in these two regions are quite steep since the electrodes are at lower temperatures than the plasma column.

2. *Melting efficiency is defined as the ratio of the heat necessary to just melt the fusion zone to the heat absorbed by the workpiece. It is a dimensionless parameter.*

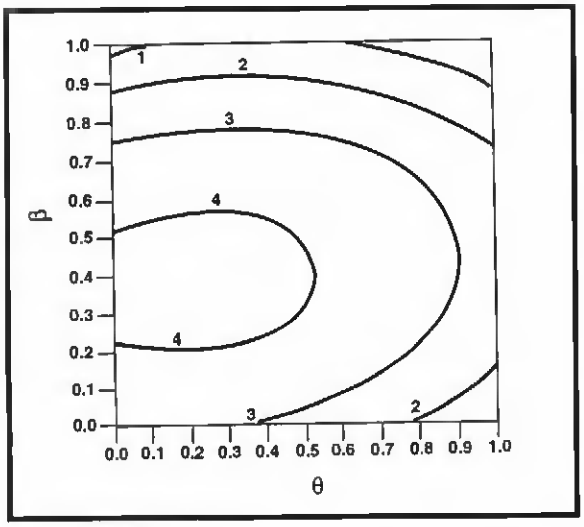

Fig. 11— Effect of independent polarity parameters on qualitative appearance rating. The parameter β represents the electrode negative fraction of the arc current. The parameter θ indicates the electrode negative duty cycle.

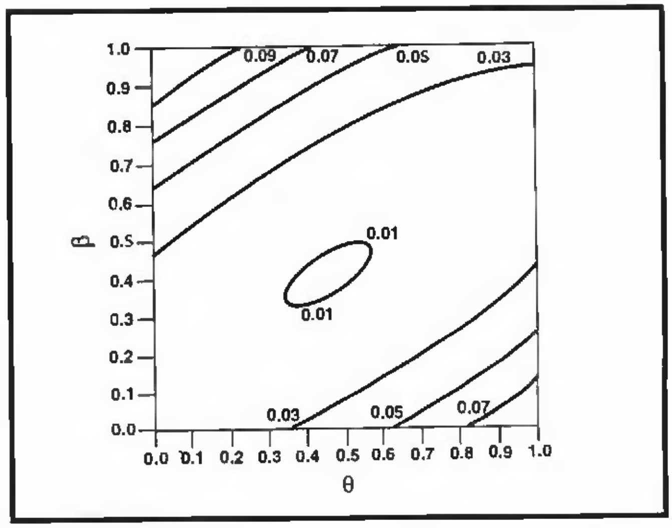

Fig. 12 — Effect of independent polarity parameters on measured surface roughness. The parameter β represents the electrode negative fraction of the arc current. The parameter θ indicates the electrode negative duty cycle.

At the anode in electrode negative polarity GTAW or PAW, ions do not enter the arc from the workpiece metal, so the current there is carried solely by electrons. In order that the resulting negative space charge be small, positive ions must be produced very close to the anode and a certain field energy is required for the production of these ions. The value of the anode fall voltage is determined by the energy requirements for this ion production (Ref. 18). Neglecting a small contribution to anode heating from the thermal energy of the electrons, the heat given to the anode, H_a, is equal to the energy gained by the incoming electrons when they are accelerated by the anode fall voltage, V_a, plus the work function energy:

$$H_a = j(V_a + \phi) \quad (9)$$

where j is the anode current density, and ϕ is the work function. The work function energy is additive because each electron neutralizes a positive metal ion in the anode material. It is believed that the incoming electrons take up almost all the energy produced in the anode fall region and transfer that energy to the anode workpiece (Ref. 2).

At the cathode in electrode negative polarity GTAW or PAW, the high current densities for welding are achieved by thermionic emission at the tip of the hot tungsten cathode. The energy for thermionic emission is believed to come from the incoming positive ions, which gain kinetic energy from acceleration in the cathode fall potential, V_c. The net heat input to the cathode, H_c, including only electronic effects, was given by Cobine:

$$H_c = j_i(V_c + V_i - \phi) - j_e\phi \quad (10)$$

where V_i is the ion ionization potential, and j_e and j_i are the electron current density and the ion current density, respectively (Refs. 2, 21). For the thermionic cathode in electrode negative polarity GTAW or PAW, substantial cooling of the tungsten by the emitting electrons occurs. Moreover, heating by the positive ions is probably low since we know the bulk of arc energy is transferred to the workpiece in electrode negative polarity.

During electrode positive polarity VPPAW, the aluminum workpiece, rather than the tungsten, must produce electrons, but the boiling point of aluminum is at a temperature below that for thermionic emission. We can see from Fig. 1A, B that the measured arc voltages during electrode positive polarity can be significantly higher than in electrode negative polarity. These higher arc voltages could be due to an increase in the anode fall voltage or the cathode fall voltage. For two reasons, it seems likely that these higher field intensities occur in the cathode fall rather than in the anode fall.

First, the temperatures at a tungsten anode are surely quite different than at an aluminum anode due to the substantial difference in melting point. Higher anode fall voltages are not expected at the tungsten since heating of the tungsten should reduce the thermal gradient in this region. Moreover, for refractory metal anodes such as tungsten, Cobine and Burger (Ref. 17) suggest that no anode fall voltage is even necessary due to the very high anode spot temperatures.

A second factor that could reduce Va is the lack of a stagnation point at the tungsten tip. In electrode negative polarity, a stagnation point exists at the center of the workpiece anode (Ref. 22), which results in a decrease in the electrical conductivity of the gas there. But in electrode positive polarity, convective flow across the tungsten tip will likely decrease the thickness of the boundary layer and the anode fall region.

These factors seem to indicate the observed voltage increase during electrode positive polarity occurs in the cathode fall region. One can see from Equation 10 that an increased cathode fall voltage may result in increased heating of the workpiece cathode. The higher arc voltages are therefore in agreement with substantial workpiece heating during electrode positive polarity.

Higher voltages in the cathode fall region are also consistent with field type emission of electrons from a relatively cold cathode, where high electric field intensities are required. Estimates in the literature of the electric field intensity based on measured fall voltages with cold cathodes indicate the magnitude may not be sufficient for field emission of electrons (Refs. 2, 18). It is thought that a layer of positive ions collecting above a thin insulating oxide on the cathode surface assists in reducing this potential barrier. Accordingly, field type emission from similar thin oxide films has been observed with $Al\text{-}Al_2O_3$ cathodes (Ref. 21). The wandering cathode spots that can be seen on the aluminum workpiece during welding are yet another distinguishing characteristic of field type emission with low boiling point metals (Refs. 2, 21).

Von Engel noted that field emission electrons contrast with thermionic electrons in that they possess a different energy distribution and that no cooling of the cathode is observed when field electrons flow from a cathode. Unlike thermionic electrons, the field electrons draw their energy from the electric field only and do not acquire any work function energy (Ref. 21). Similarly, Cobine (Ref. 2) derived an effective work function ϕ' for electrons escaping by field emission:

$$\phi' = \phi - (eE)^{1/2} \tag{11}$$

where e is the electron charge, and E is the electrostatic field. In both the von Engel and Cobine models, the energy of escaping electrons is reduced when compared with thermionic emission and less cooling of the cathode will occur. One can see from Equation 10 how decreased cooling of the cathode may result if the electron work function is reduced.

It is indicated both by higher cathode fall voltages and by an absence of cathode cooling that the production of field emission electrons may account for substantial heating of the aluminum cathode. While the physics of energy exchange in the cathode fall region is not well understood, and indeed is widely debated (Ref. 23), these results indicate that for electrode positive VPPAW, a large fraction of the arc energy is transferred to the aluminum cathode rather than to the tungsten anode.

Weld Size and Melting Efficiency

The dimensions of the fusion zone in variable polarity welding are thought to correlate with polarity balance. This is based on the common belief that polarity balance strongly affects net heat input and thereby influences melting. The results of this experiment do not support this model. The lack of correlation between weld penetration depth and arc polarity balance is illustrated in Fig. 7. One can see from the figure that although weld penetration varied significantly in this experiment, polarity balance is not the root cause.

Micrographs of typical fusion zone shapes and their corresponding experimental conditions are given in Fig. 8A, B. Despite the high fraction of electrode negative polarity balance, the weld in Fig. 8B is substantially smaller than the weld in Fig. 8A. The important correlation of weld penetration and cross-sectional area with net input power can be inferred from these two figures. The net power absorbed by the weld in Fig. 8A is almost 50% greater than the power absorbed by the weld in Fig. 8B.

The variation in fusion zone size in the experiment can be explained by the substantial fluctuations in net input power that occurred. Figure 9 illustrates the strong dependence of measured weld size on the power transferred to the workpiece. Clearly the total power in the arc and the resulting fraction absorbed are the factors that determine melting in VPPAW.

The poor weld penetration with electrode positive polarity that has been described by other researchers is real (Ref. 1) and should be considered here. It is clear from Fig. 7 that relatively deep penetration welds were made at very low levels of electrode negative polarity power. Certainly the edge weld geometry in this experiment is atypical and is known to create two-dimensional heat flow rather than the three-dimensional heat flow that occurs in a flat plate. But two-dimensional heat flow conditions cannot account for the penetration invariance with polarity, since all of the welds should have a similar heat flow geometry.

The decreased penetration and melting that typically occurs during electrode positive polarity welding is more logically explained by decreased power density rather than decreased power. A broader energy distribution on the workpiece during electrode positive polarity could cause wider welds as well as a lower melting efficiency. Vilkas (Ref. 1) reported that the GTAW arc spatial distribution on a water-cooled copper workpiece was substantially wider for a electrode positive polarity arc than for a electrode negative polarity arc. Similarly, Martinez, *et al.* (Ref. 12), found for the VPPAW process that constricting the arc through helium additions to the shielding gas results in increased melting of the workpiece metal. In this manner a noticeable change in fusion zone dimensions could occur even if the net power remains the same.

Perhaps in this experiment, the edge weld geometry served to concentrate the arc within a narrow region. If the arc spatial extent was restricted by the edge weld geometry, no variation in melting with polarity balance would be observed. In addition, the stiff plasma arc and the helium shielding may both have served to prevent the arc from broadening in this experiment. Measurements of VPPAW arc efficiency for flat plates would help in confirming this explanation.

The strong correlation between melting and heat input seen in Fig. 9 is due to the fact that weld travel speed was kept the same for all of these welds. Under these constraints, incremental changes in heat input will be closely followed by comparable changes in melting. The slightly increasing slope in Fig. 8 is due to the beneficial effect of power on melting efficiency[2]. The dimensionless Rykalin parameter (Ref. 24) is known to closely correlate with melting efficiency:

$$Ry = \frac{q_i \upsilon}{\alpha^2 \delta h} \tag{12}$$

where q_i = net power into the workpiece; υ = travel speed; α = thermal diffusivity at the liquidus temperature; δh = enthalpy of melting; A = weld cross-sectional area.

One can see that Ry will necessarily increase as the power to the part is increased. Because of this, a rising melting efficiency and a nonlinear slope is expected for the welds in Fig. 7.

The dramatic increase in melting efficiency that occurred in the experiment can be seen in Fig. 10. The measured melting efficiencies ranged from 0.05 to 0.34. The highest values are somewhat low compared to the maximum value of 0.48, which should be obtainable for the two-dimensional heat flow typical in edge welds (Ref. 10). The peak melting efficiency values are likely low because the thermal diffusivity of pure Al is quite high. It is expected that with faster travel speeds and higher values of Ry, optimum (*i.e.*, maximum) melting efficiency could be obtained.

It is also apparent that compared with the electrode negative polarity GTA and PA welds represented by the curve in Fig. 10, the melting efficiencies for most of the VPPAW welds are increasing faster with Ry. The discrepancy between the present data and the model represented (Ref. 25) by the curve in Fig. 10 is thought to be due to the tangible effect of current pulsation. In an earlier study with pulsed PAW and GTAW, Fuerschbach and Knorovsky (Ref. 10) found that current pulsation greatly improved melting efficiency compared to continuous power welds made at the same travel speed. The variable polarity welds made in the present study are pulsed welds since the current was cycled at 50 Hz, with variable duty cycles — Table 2. While Ry has been shown to be a strong indicator of melting efficiency, it does not take into account the temporal effects of power pulsation. The rapid increase for the VPPAW welds relative to the continuous power welds shown in Fig. 10 indicates that variable polarity can enhance melting efficiency for low values of Ry.

Cathodic Cleaning

The importance of cathodic cleaning in the fusion welding of aluminum is readily apparent when joining this unique material. When the oxide is effectively removed in the arc, the welds are remarkably smooth and glossy in appearance. In contrast, even with robust preweld chemical cleaning techniques, aluminum welds will be unsatisfactory cosmetically if the oxide is not adequately removed by cathodic cleaning in the arc. Preweld cleaning is usually insufficient because the aluminum oxide quickly reforms on the surface after exposure to the shop atmosphere.

The presence of aluminum oxide in the fusion zone during postweld inspection usually is indicated by weld pools that are rough and dull in appearance. Inadequate oxide removal also is denoted by welds that appear to have solidified in a viscous condition. That is, the presence of excessive aluminum oxide in the weld pool is often seen to decrease weld pool fluidity. While important in aluminum fabrication, such qualitative indicators are not usually specified as primary criteria for visual inspection in aluminum welding codes (Ref. 26). Qualitative measures of oxide removal also are difficult to apply in an engineering study.

Few techniques are available to quantitatively assess the effectiveness of oxide removal after a weld has been completed. Some attempts have been made to measure the geometric extent of the cleaned region adjacent to the weld (Refs. 1, 9). However, a correlation between oxide removal from the fusion zone and the dimensions of the cleaned area has not been demonstrated. Measurements such as these were not feasible in this study since the edge weld geometry limits the cleaned region. Real-time measurements of cleaning appear impractical since spectroscopic analysis of the arc during VPPA welding of aluminum by Pang, *et al.* (Ref. 3), found no correlation between aluminum intensity lines and oxide removal rates. More sophisticated postweld analytical techniques to measure the thickness of the weld oxide, such as Auger electron spectroscopy, are feasible, but would be prohibitively expensive for the large number of welds that would need to be examined.

While the quantitative assessment of cleaning effectiveness is difficult, there were welds made in this study that were clearly more cosmetically appealing than others. Two techniques, one qualitative and the other quantitative, proved valuable in characterizing cathodic cleaning.

Using a subjective visual approach, all of the welds were graded on a scale from 1 to 4, where 4 is an ideal weld and 1 is a poor and unsatisfactory weld. Figure 11 shows the dependence of this qualitative appearance ranking vs. the independent polarity balance parameters β and θ. The contour plot indicates that optimum cleaning occurred for levels of β between 0.2 and 0.5 and for levels of θ less than 0.5. Not surprisingly, these levels correspond to conditions of substantial electrode positive polarity power. If we compare these values of β and θ with the corresponding process parameters in Table 2, we can see that the extent of electrode positive polarity duration was quite important for optimum cleaning. Moreover, neither electrode negative nor electrode positive current amplitude were significant in promoting oxide removal.

The trends evidenced by these subjective appearance rankings are supported by quantitative surface roughness measurements made on the same welds. Figure 12 shows the correlation between the fusion zone surface roughness measurements and the independent polarity balance parameters β and θ. The surface roughness values given in Fig. 12 are really a measure of specular reflection and therefore represent the weld's degree of glossiness. Smoother welds will be glossier and have lower measured values. It is thought that the smoothest welds represent low viscosity, minimal oxide, and conditions of optimum cathodic cleaning. The contour plot indicates that optimum cleaning occurred for levels of both β and θ between about 0.3 and 0.5. The effect of β and θ on surface roughness is reasonably consistent with the qualitative assessment results shown in Fig. 11.

It is interesting to note that for the conditions in Table 2 that correlate with optimum cleaning in Figs. 11 and 12, the electrode negative and electrode positive current levels are close to the balanced wave levels that have been traditionally used for successful aluminum welding. Before the advent of solid state electronic control and variable polarity features, AC power supplies were designed to give equal amplitudes for electrode negative and electrode positive polarity current. A qualitative study by Sager, *et al.* (Ref. 27), found that balanced wave power supplies are actually preferred for ideal cathodic cleaning. Similarly, in this study, excellent quality welds were obtained for all of the conditions close to a 50% polarity balance for current and duration.

However, it should be mentioned that a balanced current wave does not really result in balanced power. Even when both β and θ are equal to 0.5, the power balance is not equal. Figure 3 indicates that this condition results in a polarity balance of 0.35. Nonetheless, it is surprising to find that some degree of electrode negative polarity is required for optimum cathodic cleaning. Perhaps excessive electrode positive polarity results in too much removal of the oxide and the arc becomes unstable. A large cathodically cleaned region adjacent to the weld may be a sign of excessive arc wandering and a precursor to arc instability and unsatisfactory welds. Until we develop a practical technique to quantitatively measure aluminum oxide removal, our understanding of cathodic cleaning will remain qualitative and incomplete.

Summary and Conclusions

The lack of correlation between polarity balance and the measured VPPAW arc efficiencies indicate that heat input to the workpiece is not strongly affected by polarity. It seems reasonable that the design and application of variable polarity power supplies should emphasize the optimization of cathodic cleaning effects or to minimize tungsten degradation rather than the selection of negative polarity current balance, since polarity is not a true indicator of arc energy transfer.

For the conditions of this study, the following were found:

1) The independent polarity balance parameters (β and θ) used in the design of this experiment were found to be effective in obtaining a wide range of measured electrode negative and electrode positive polarity power.

2) For the 1100 Al edge welds examined here, VPPAW arc efficiency ranged from 0.41 to 0.62, and measured arc efficiencies did not correlate with variations in polarity balance.

3) Net heat input to the workpiece and arc output energy did not correlate with polarity balance. It was found that both increased at low negative polarity balance as a result of increased arc voltages.

4) The overall consistency in measured arc efficiency, despite significant changes in polarity, has been attributed to increased energy transfer to the aluminum cathode as the cathode fall voltage rises during the electrode positive polarity cycle.

5) Substantial heating of the aluminum workpiece during electrode positive polarity is explained by field type emission of electrons from a low boiling point cathode with a thin oxide film. Unlike thermionic emission, field emission electrons do not cool the cathode.

6) Fusion zone size was found to solely depend on the net input power. It

is postulated that the edge weld joint design prevents the arc spot size from broadening at increased positive polarity balance and thereby decreasing power density.

7) The degree of oxide removal varied widely among the welds in the experiment. Cathodic cleaning was best with levels of β and θ that yielded conditions of substantial electrode positive polarity power.

8) Levels of β and θ that produced optimum cathodic cleaning were identified. For these welds, some small degree of electrode negative polarity power was required to achieve the ideal cleaning conditions.

Acknowledgments

The author wishes to express his sincere appreciation for the fine technical contributions of Jim Bullen, Alice Kilgo and Tony Romero. I would also like to thank Jerry Knorovsky for his constructive comments and insightful guidance during the preparation of the manuscript. This work was performed at Sandia National Laboratories, which is supported by the U.S. Department of Energy under contract number DE-AC04-94AL85000.

References

1. Vilkas, E. P. 1967. Square-Wave Welding. *Trans. IEEE IGA* 3(6): 525–530.

2. Cobine, J. D. 1941. *Gaseous Conductors*, McGraw Hill: New York.

3. Pang, Q., Pang, T., Nunes, A. C., McClure, J. 1994. Workpiece cleaning during variable polarity plasma arc welding of aluminum. ASME, *Journal of Engineering for Industry* 116(11): 463–466.

4. Guile, A. E. 1979. Processes at arc cathode roots on nonrefractory metals having films of their own oxide. *Arc Physics and Weld Pool Behavior.* The Welding Institute: London, pp. 79–86.

5. Druyvesteyn, M. J. 1936. Electron emission of the cathode of an arc. *Nature* 137:580.

6. Cobine, J. D. 1949. The Nature of the Arc, Welding Research Council, No. 2.

7. Correy, T. B. 1962; Method For Obtaining An Improved Weld In Inert Arc Welding. Patent No. 3068352.

8. VanCleave, B. P. 1980. Keyhole plasma arc welding of aluminum. *Welding Technology for The Aerospace Industry*, Las Vegas, Nevada.

9. Okada, T., Iwamoto, Y., Wakino, Y., Yamamota, H., and Okazaki, K. 1982. The effects of polarity in TIG arc welding of aluminum with thryistor controlled power source. *J. Light Met. Weld. Constr.* 16 (12):537–543.

10. Fuerschbach, P. W., and Knorovsky, G. A. 1991. A study of melting efficiency in plasma arc and gas tungsten arc welding. *Welding Journal* 70(10): 28-s to 297-s.

11. Giedt, W. H., Tallerico, L. N., and Fuerschbach, P. W. 1989. GTA welding efficiency: calorimetric and temperature field measurements. *Welding Journal* 68(1): 28-s to 32-s.

12. Martinez, L. F., Matlock, C., Marques, R. E., McClure, J. C., and Nunes, A. C. 1994. Effect of weld gases on melt zone size in VPPA welding of Al 2219. *Welding Journal* 73(10):51.

13. Stover, J. C. 1990. *Optical Scattering Measurement Analysis*, McGraw Hill: New York.

14. Dupont, J. N., and Marder, A. R. 1995. Thermal efficiency of arc welding processes. *Welding Journal* 74(12): 406-s to 416-s.

15. Smartt, H. B., Stewart, J. A., and Einerson, C. J. 1985. Heat transfer in gas tungsten arc welding. *ASM International Welding Congress.* ASM, Toronto, Canada.

16. Tomsic, M., and Barhorst, S. 1984. Keyhole plasma arc welding of aluminum with variable polarity power. *Welding Journal* 63(2): 25–32.

17. Cobine, J. D., and Burger, E. E. 1955. Analysis of Electrode Phenomena in the High Current Arc. *J. Appl. Phys.* 26(7):895–900.

18. Somerville, J. M. 1959. *The Electric Arc.* Methuen & Co., London.

19. Schoeck, P. A., and Eckert, E. R. G. 1961. Experiments on the transpiration cooled anode of an electric arc. *Heat Transfer and Fluid Mechanics Inst.* Stanford Univ. Press, USC.

20. Incropera, F. P., and Dewitt, D. P. 1981. *Fundamentals of Heat Transfer*, John Wiley & Sons, New York.

21. VonEngel, A. 1965. *Ionized Gases*, Clarendon Press, Oxford.

22. Schoeck, P. A., and Eckert, E. R. G. 1961. An investigation of anode heat transfer in high intensity arcs. *Ionization Phenomena in Gases*, North Holland Publishing, Munich.

23. Hoyaux, M. F. 1968. *Arc Physics*, Springer-Verlag, New York.

24. Fuerschbach, P. W. 1996. Measurement and prediction of energy transfer efficiency in laser beam welding. *Welding Journal* 75(1): 24-s to 34-s.

25. Fuerschbach, P. W. 1995. A dimensionless parameter model for arc welding processes. *4th Intl. Conf. on Trends in Welding Research.* ASM Intl., Gatlinburg, Tenn.

26. AWS. 1990. *Structural Welding Code — Aluminum*, ANSI/AWS D1.2-90, American Welding Society, Miami, Fla.

27. Sager, R. K., Michnuk, P. R., and Mahan, G. W. 1976. *Evaluate and Develop Automatic AC TIG Welding of Aluminum Pipe, Alcoa Laboratories*, U.S. Govt. contract W-7405-eng-26.